Extremely Stable Metal-Encapsulated $AlPb_{10}^+$ and $AlPb_{12}^+$ Clusters: Mass-Spectrometric Discovery and Density Functional Theory Study

S. Neukermans,[1] E. Janssens,[1] Z. F. Chen,[2] R. E. Silverans,[1] P. v. R. Schleyer,[2] and P. Lievens[1,*]

[1]*Laboratorium voor Vaste-Stoffysica en Magnetisme, Katholieke Universiteit Leuven, Celestijnenlaan 200D, B-3001 Leuven, Belgium*

[2]*Centre for Computational Chemistry, University of Georgia, Athens, Georgia 30602, USA*

(Received 15 December 2003; published 19 April 2004)

We report the experimental discovery of extremely stable metal-encapsulated superatom clusters of a group IVA element: $AlPb_{10}^+$ and $AlPb_{12}^+$. *Ab initio* density functional geometry optimizations at the B3LYP/LANL2DZ level result in a perfect icosahedron with an exceptionally large HOMO-LUMO gap of 3.1 eV for $AlPb_{12}^+$, and a related structure with D_{4d} symmetry for $AlPb_{10}^+$, with a HOMO-LUMO gap of 2.6 eV. Their high stability is attributed to the reinforcing influence of the most favorable closed-packed structure and optimally filled electron shells.

DOI: 10.1103/PhysRevLett.92.163401 PACS numbers: 36.40.–c, 61.46.+w

The quest for chemically (quasi)inert cluster species that could serve as *artificial atoms* for the construction of nanostructured materials is a leading thread in current research [1–3]. Symmetric clusters with unique physicochemical properties may be ideal building blocks for tailored nanomaterials. Aside from highly symmetric systems such as C_{60} [4], binary clusters are well suited for this purpose, since they offer the inherent possibility of altering cluster properties nearly at will by manipulating size, shape, and composition [5].

Metal-encapsulated Si and Ge clusters are well-studied examples, experimentally [6] and computationally [5,7–13]. Their optoelectronic properties make them attractive candidates for the development of nanostructured devices [7,14]. Recently, some of their heavier congeners, bimetallic Pb-based clusters, were identified mass spectrometrically [15,16]. In particular the 13-atom icosahedra with an encapsulated atom are particularly intriguing [9,17–20]. While many such cluster icosahedra have been predicted computationally [7,9,21], very few have been investigated and identified experimentally [15,22,23].

We report the discovery and mass spectral characterization of gas-phase Al-doped Pb_n^+ clusters. Prominent abundances in the mass spectra are compelling evidence for a considerably enhanced stability of $AlPb_{12}^+$ and $AlPb_{10}^+$. Geometry optimizations at the B3LYP/LAN2DZ level of theory reveal that $AlPb_{12}^+$ is a perfect icosahedron, and that $AlPb_{10}^+$ is a bicapped tetragonal antiprism. Both structures encapsulate the Al atom in a highly coordinated central position.

The clusters were produced with a dual-target dual-laser vaporization source [24]. A 7 bar He carrier gas pressure was used and a conical nozzle (10° opening angle and 1 mm diameter) terminated the formation chamber. Cationic clusters are mass analyzed in a reflectron time-of-flight mass spectrometer. The mass abundance spectrum for $AlPb_n^+$ clusters is shown in Fig. 1(a). The mass spectra of pure Al_n^+ and Pb_n^+, produced with the same cluster settings, are shown in Fig. 1(b) and 1(c), respectively (same vertical scale). The peak amplitudes for pure Al_n^+ and Pb_n^+ are significantly reduced in Fig. 1(a). In contrast, Pb_n clusters doped with a single Al atom ($AlPb_n^+$ with $n = 6 – 13$) are observed in high abundance. The highly prominent $AlPb_{12}^+$ peak and, to a lesser extent, that of $AlPb_{10}^+$ are striking.

Do the abundances observed in the mass spectra reflect the relative stability of the clusters produced under the

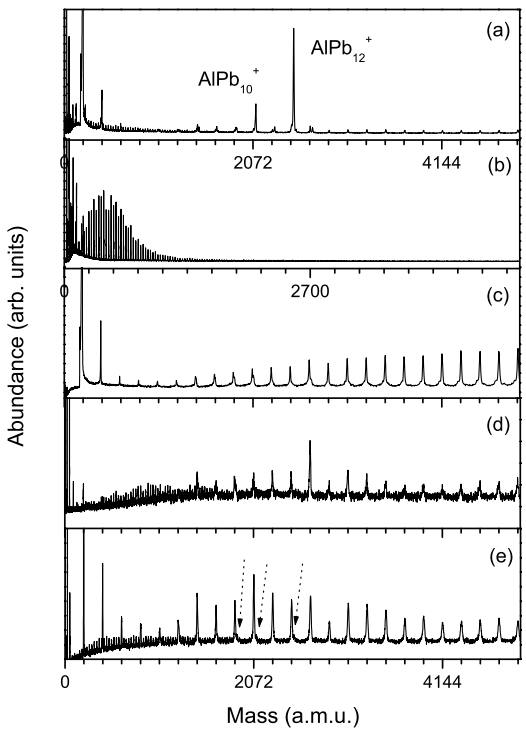

FIG. 1. (a) Mass abundance spectrum of mixed $AlPb_n^+$ clusters, showing the extremely enhanced stability of $AlPb_{10}^+$ and $AlPb_{12}^+$. (b) Pure Al_n^+ clusters. (c) Pure Pb_n^+ clusters. Mass abundance spectra of neutral mixed $AlPb_n$ clusters, ionized using 6.4 eV (d) and 7.9 eV (e) photon energy, respectively.

 0031-9007/04/92(16)/163401(4)$22.50

experimental conditions employed [25]? When condensation and evaporation processes are in equilibrium before the adiabatic expansion of the mixed monomer-cluster vapor, the resulting abundances are determined thermodynamically and, consequently, are sensitive to binding energies. This is expected in, e.g., hot oven sources. The violent formation processes in laser vaporization sources are much more poorly understood. However, the cluster size distribution is known to be very sensitive to the parameters of the source (metal vapor density, gas pressure, source dimensions); in (exceptional) extreme size-dependent cases, the mass spectra reflect high stability. The buckminsterfullerenes C_{60} and C_{70} [4] and small binary clusters Li_6C and Na_6Pb [26–28] are examples.

The abundance of the neutral species was probed using photoionization with low fluence laser light ($<100\ \mu J/cm^2$) stemming from an ArF (6.4 eV) or an F_2 (7.9 eV) excimer laser. In the resulting mass spectra, shown in Figs. 1(d) and 1(e), respectively, peaks corresponding to pure Al_n and Pb_n clusters are observed clearly. In contrast with the cations [Fig. 1(a)], no peaks corresponding to neutral $AlPb_n$ clusters are detected for ionization with 6.4 eV [Fig. 1(d)]. The spectrum recorded using 7.9 eV photons [Fig. 1(e)] shows very small intensities corresponding to $AlPb_9$, $AlPb_{10}$, and $AlPb_{12}$ [dotted arrows in Fig. 1(e)].

Based on the experience in metal-encapsulated Si and Ge clusters, Zintl ions [29,30] and Pb clusters [31], various possible isomers of $AlPb_{12}^+$ and $AlPb_{10}^+$ (Figs. 2 and 3) were optimized using the GAUSSIAN98 [32] package in given symmetries at the B3LYP/LANL2DZ level. Frequency analyses determined the nature of the stationary points. The mode following of the first imaginary frequency (if present) leads to the true minimum. Highest occupied molecular orbital (HOMO) lowest unoccupied molecular orbital (LUMO) gaps were calculated as a relative measure for the closed electronic shell character and compared with other calculations in the literature [7,9,10]. The HOMO-LUMO values computed using other levels of theory can be found in Ref. [33].

The hybrid density functional computations show that the I_h symmetrical $AlPb_{12}^+$, in which the 12 lead atoms symmetrically encapsulate the aluminum dopant, is the most stable isomer. It is 1.96 eV (40 kcal/mol) lower in energy than the second best isomer. The relative energies of the different isomers are listed in Table I. The extremely large HOMO-LUMO gap of about 3.1 eV is striking. The bicapped tetragonal antiprism with D_{4d} symmetry is the $AlPb_{10}^+$ global minimum; other isomers are at least 0.77 eV (16 kcal/mol) higher in energy. This D_{4d} structure also has a very large 2.6 eV HOMO-LUMO gap. The relative energies of the different isomers for $AlPb_{10}^+$ are listed in Table II.

The exceptionally large HOMO-LUMO gaps of the highly symmetric D_{4d} ($AlPb_{10}^+$) and I_h ($AlPb_{12}^+$) suggest very favorable *magic* electronic structures. We investigated this in detail for $AlPb_{12}^+$. The $3s^2 3p^1$ valence electrons of the aluminum atoms in clusters are delocalized [34]; when electron shells are closed, this results in size-dependent stability features. The situation is less straightforward for lead clusters. Even though all four lead atom valence electrons ($6s^2 6p^2$) may delocalize, the stability of lead clusters is determined by the interplay between geometrical (close-packed) and electronic (closed shell) structural features [31].

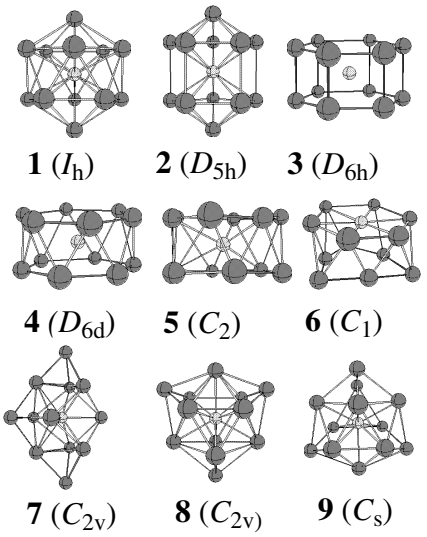

FIG. 2. $AlPb_{12}^+$: B3LYP/LANL2DZ optimized structures.

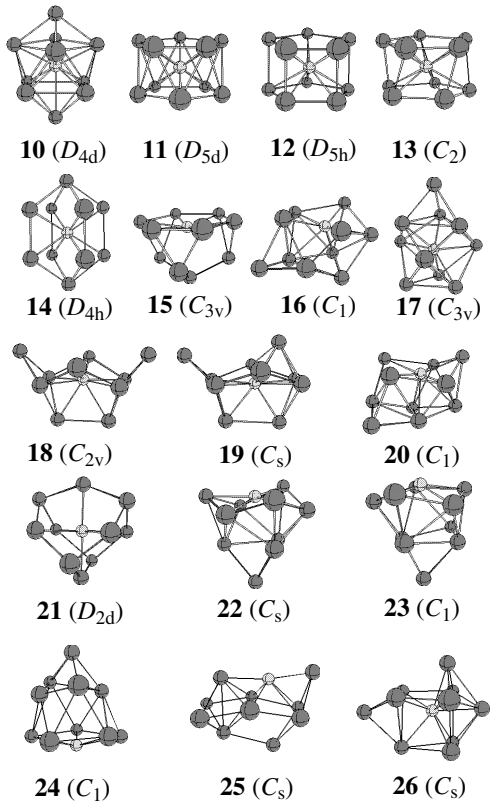

FIG. 3. $AlPb_{10}^+$: B3LYP/LANL2DZ optimized structures.

TABLE I. Total energies, zero-point energies (ZPE), numbers of imaginary frequency, structures resulting from mode following of the first imaginary frequency, and relative energies (with ZPE correction) of various possible isomers of $AlPb_{12}^+$.

	Symm.	E_{tot} (au)	ZPE (eV)	NIMAG	Mode following	E_{rel} (eV)
1	I_h	−43.922 44	0.18	0		0.00
2	D_{5h}	−43.844 93	0.16	3	**1**	2.34
3	D_{6h}	−43.74 141	0.13	9	**1**	5.45
4	D_{6d}	−43.80 850	0.14	6	**5**	3.42
5	C_2	−43.81 913	0.16	3	**6**	3.11
6	C_1	−43.84 429	0.16	0		2.36
7	C_{2v}	−43.85 780	0.17	0		1.96
8	C_{2v}	−43.85 056	0.16	1	**9**	2.16
9	C_s	−43.85 061	0.16	0		2.16

The orbitals of the I_h ground state reveal the degree to which the valence electrons of the constituent atoms in $AlPb_{12}^+$ are delocalized. All 50 valence electrons occupy 25 molecular orbitals (MO's) delocalized over the entire cluster volume. The MO energies, symmetries, and symmetry patterns (one for each of the degenerate occupied levels) are shown in Fig. 4. Because of the high (almost spherical) I_h symmetry, the orbitals strongly resemble the spherical harmonics, but with significant variations. A $1s$ type valence MO (A_g symmetry) holding two electrons ($1s^2$) is lowest. In spherical symmetry, this would be followed by a triply degenerate $1p$ type (T_{1u}) $1p^6$ shell, a pentuply degenerate $1d^{10}$ shell (H_g), a heptuply degenerate $1f^{14}$ shell, and a ninefold degenerate $1g^{18}$ shell.

TABLE II. Total energies, zero-point energies, numbers of imaginary frequency, structures resulting from mode following of the first imaginary frequency, and the relative energies of various possible isomers of $AlPb_{10}^+$.

	Symm.	E_{tot} (au)	ZPE (eV)	NIMAG	Mode following	E_{rel} (eV)
10	D_{4d}	−36.87 551	0.16	0		0.00
11	D_{5d}	−36.81 040	0.14	3	**13**	1.96
12	D_{5h}	−36.80 329	0.15	1	**13**	2.18
13	C_2	−36.82 554	0.15	0		1.51
14	D_{4h}	−36.77 263	0.13	1	**10**	3.09
15	C_{3v}	−36.73 377	0.11	7	**16**	4.26
16	C_1	−36.84 470	0.15	0		0.93
17	C_{3v}	−36.82 608	0.15	2	**10**	1.49
18	C_{2v}	−36.79 043	0.14	1	**19**	2.57
19	C_s	−36.80 057	0.14	1	**20**	2.26
20	C_1	−36.84 470	0.15	0		0.93
21	D_{2d}	−36.75 400	0.11	7	**22**	3.65
22	C_s	−36.82 697	0.14	1	**23**	1.46
23	C_1	−36.85 013	0.15	0		0.77
24	C_1	−36.83 917	0.15	0		1.10
25	C_s	−36.81 540	0.15	0		1.81
26	C_s	−36.84 519	0.15	0		0.92

Although these orbitals would hold a total of 50 electrons, they do not constitute the electronic structure of $AlPb_{12}^+$.

In I_h symmetry, the $l = 3$ ($1f$) level splits into threefold (T_{2u}) and fourfold (G_u) degenerate levels. The $l = 4$ ($1g$) level splits into a fivefold (H_g) and a fourfold (G_g) degenerate level. More importantly, long before the first spherical progression is complete, the second set begins and blends into the first: $2s$ ($2A_g$), $2p$ ($2T_{1u}$). Consequently, 42 electrons ($2 + 6 + 10 + 14 + 10$) from the first spherical set and 8 electrons ($2 + 6$) from the second constitute the 50 valence electrons of $AlPb_{12}^+$.

While the computations clearly show that 50 electrons correspond to the electronic magic number identified for spherical aromatic systems [35], this count does not appear in simple shell models where 2, 8, 18/20, 34/40, 58, and 68 valence electrons constitute closed shells [36]. The 50 electron shell closing originates physically from the crystal-field splitting of the high angular momentum (high l) spherical levels according to the structural symmetry of the cluster [34,37]. The radial orbitals that point towards the positively charged lead atom centers are favored in energy while the tangential MO's with maximum density between the atoms are less favorable energetically [38]. The $1g$ splitting results in a very pronounced energy gap (3.1 eV) at the 50 electron occupancy. The LUMO level consists of a quadruply degenerate $1g$ orbital set (G_g) nearly isoenergetic with the $3s$ (A_g) level.

The same rationalization holds true for $AlPb_{10}^+$ with D_{4d} symmetry, which has 21 delocalized orbitals

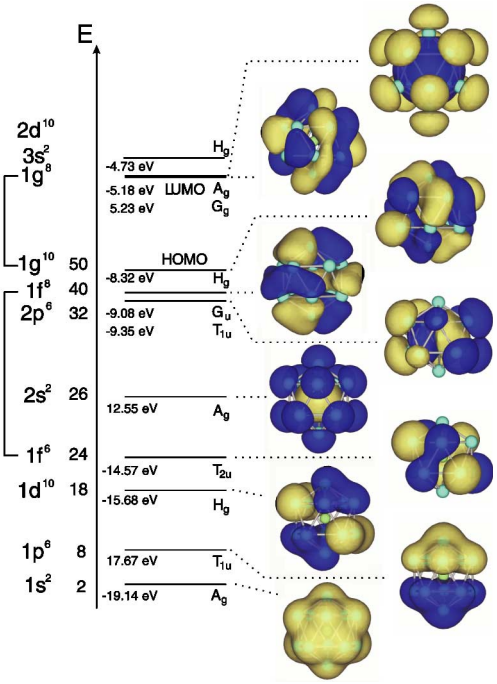

FIG. 4 (color online). Energy level scheme and orbitals (one for each set) for the $AlPb_{12}^+$ ground state (**1**, I_h) at B3LYP/LANL2DZ.

containing 42 electrons (see [33]). As only double degeneracy is possible, the p-, d-, f-, and g-type degeneracies are lifted, and orbitals with symmetry along the fourfold axis are favored. As a result, the high HOMO-LUMO gap of 2.63 eV and a 42 electron closed shell configuration can be interpreted as stemming from a crystal-field splitting of the $1g$ shell. The HOMO is a $1g$-derived (A_1) orbital oriented along the fourfold axis. The total of 42 electrons results from 34 electrons ($1s^2 + 1p^6 + 1d^{10} + 1f^{14} + 1g^2$) from the first spherical set and 8 electrons ($2p^2 + 2p^6$) from the second set that blends into the first.

The magic electronic character for both $AlPb_{10}^+$ and $AlPb_{12}^+$ is confirmed by the nucleus independent shift calculation values, revealing the aromatic character of $AlPb_{10}^+$ (ca. -26 ppm near the cage center) and $AlPb_{12}^+$ (-20 ppm), as well as the isoelectronic Pb_{10}^{2-} (-24.9 ppm) and Pb_{12}^{2-} (-10.8 ppm) cages [39]. Well delocalized electrons in aromatic systems are characterized by enhanced stabilization energies, which leads in three-dimensional systems to *magic* clusters. The highly aromatic character of Pb_{10}^{2-} and Pb_{12}^{2-}, and their large cavities and electronic structures that host an aluminum atom effectively, supports the description of $Al@Pb_{10}^+$ and $Al@Pb_{12}^+$ as magic clusters.

In conclusion, we reported the experimental discovery of unusually stable binary $AlPb_{10}^+$ and $AlPb_{12}^+$ clusters and the computational demonstration that their preferred symmetric endohedral structures encapsulate an aluminum ion. The observed stability and the large computed HOMO-LUMO gaps are due to the combined effect of highly symmetric close-packed structures, closed crystal-field split electron shell configurations, and a three-dimensional aromatic character. These species should be very promising potential building blocks for cluster assembled materials.

This work is supported by the Fund for Scientific Research–Flanders (FWO), by the Flemish Concerted Action (GOA), and by the Belgian Interuniversity Poles of Attraction (IAP) programs. National Science Foundation (CHE-0209857) supported the work in Georgia. S. N. and E. J. thank the FWO for financial support.

Note added in proof.—Following completion of this work we learned about a theoretical investigation of $X_{10}M$ clusters (X = Si, Ge, Sn, Pb; M = Ni, Pd, Pt) [40] and the synthesis of $[Pt@Pb_{12}]^{2-}$ compounds [41].

*Electronic address: Peter.Lievens@fys.kuleuven.ac.be

[1] J. Li *et al.*, Science **299**, 864 (2003).
[2] X. Gong, Phys. Rev. B **56**, 1091 (1997).
[3] K. Ho *et al.*, Nature (London) **392**, 582 (1998).
[4] H. Kroto *et al.*, Nature (London) **318**, 162 (1985).
[5] V. Kumar and Y. Kawazoe, Phys. Rev. Lett. **88**, 235504 (2002), and references therein.
[6] M. Ohara *et al.*, Chem. Phys. Lett. **371**, 490 (2003).
[7] V. Kumar and Y. Kawazoe, Appl. Phys. Lett. **80**, 859 (2002), and references therein.
[8] S. Khanna, B. Rao, and P. Jena, Phys. Rev. Lett. **89**, 16803 (2002).
[9] J. Lu and S. Nagase, Chem. Phys. Lett. **372**, 394 (2003).
[10] V. Kumar and Y. Kawazoe, Appl. Phys. Lett. **83**, 2677 (2003).
[11] T. Miyazaki, H. Hiura, and T. Kanayama, Phys. Rev. B **66**, 121403 (2002), and references therein.
[12] F. Hagelberg, C. Xiao, and W. Lester, Phys. Rev. B **67**, 035426 (2003).
[13] Z. Chen *et al.*, J. Am. Chem. Soc. **125**, 15 507 (2003).
[14] E. Honea *et al.*, Nature (London) **366**, 42 (1993).
[15] X. Zhang *et al.*, Rapid Commun. Mass Spectrom. **15**, 2399 (2001).
[16] X. Xing *et al.*, Rapid Commun. Mass Spectrom. **17**, 1411 (2003).
[17] S. Khanna and P. Jena, Phys. Rev. Lett. **69**, 1664 (1992).
[18] X. Gong and V. Kumar, Phys. Rev. Lett. **70**, 2078 (1993).
[19] J. Jellinek and E. Krissinel, Chem. Phys. Lett. **258**, 283 (1996).
[20] B. Rao and P. Jena, J. Chem. Phys. **115**, 778 (2001).
[21] P. Pyykko and N. Runeberg, Angew. Chem., Int. Ed. Engl. **41**, 2174 (2002).
[22] X. Li and L. Wang, Phys. Rev. B **65**, 153404 (2002).
[23] X. Li *et al.*, Angew. Chem., Int. Ed. Engl. **41**, 4786 (2002).
[24] W. Bouwen *et al.*, Rev. Sci. Instrum. **71**, 54 (2000).
[25] S. Bjornholm and J. Borggreen, Philos. Mag. B **79**, 1321 (1999), and references therein.
[26] P. Schleyer *et al.*, J. Am. Chem. Soc. **105**, 5930 (1983).
[27] P. Lievens *et al.*, Eur. Phys. J. D **9**, 289 (1999).
[28] C. Yeretzian, U. Rothlisberger, and E. Schumacher, Chem. Phys. Lett. **245**, 475 (1995).
[29] C. Schrodt, F. Weigend, and R. Ahlrichs, Z. Anorg. Allg. Chem. **628**, 2478 (2002).
[30] C. Xiao, F. Hagelberg, and W. Lester, Phys. Rev. B **66**, 075425 (2002).
[31] J. Doye and S. Hendy, Eur. Phys. J. D **22**, 99 (2003), and references therein.
[32] M. Frisch *et al.*, GAUSSIAN98 (Revision A.1) (Gaussian, Inc., Pittsburgh, PA, 1998).
[33] See EPAPS Document No. E-PRLTAO-92-058413 for the molecular orbitals and HOMO-LUMO energy gaps for $AlPb_{10}^+$ and $AlPb_{12}^+$. A direct link to this document may be found in the online article's HTML reference section. The document may also be reached via the EPAPS homepage (http://www.aip.org/pubservs/epaps.html) or from ftp.aip.org in the directory /epaps/. See the EPAPS homepage for more information.
[34] K. Schriver *et al.*, Phys. Rev. Lett. **64**, 2539 (1990).
[35] A. Hirsch, Z. Chen, and H. Jiao, Angew. Chem., Int. Ed. Engl. **39**, 3915 (2000).
[36] W. deHeer, Rev. Mod. Phys. **65**, 611 (1993).
[37] H. Cheng, R. Berry, and R. Whetten, Phys. Rev. B **43**, 10 647 (1991).
[38] H. Bethe, Ann. Phys. (Leipzig) **3**, 133 (1929).
[39] P. Schleyer and H. Jiao, Pure Appl. Chem. **68**, 209 (1996).
[40] V. Kumar, A. Singh, and Y. Kawazoe, Nano Lett. **4**, 677 (2004).
[41] E. Esenturk, J. Fettinger, Y. Lam, and B. Eichhorn, Angew. Chem., Int. Ed. Engl. **43**, 2132 (2004).